2026 IEEE International Conference on Robotics and Automation (ICRA 2026)
June 1-5, 2026. Vienna, Austria

Design and Implementation of Elastic Structure Preserving Vibration Suppression Control for Flexible Link Robots using IMU Measurements

Alexander Kitzinger[1] and Hubert Gattringer[1] and Andreas Müller[1]

***Abstract*— Elastic lightweight manipulators offer multiple benefits but suffer from increased structural flexibility, making them susceptible to vibrations and thus requiring dedicated control concepts for vibration suppression. Based on a lumped element model formulation, a method called elastic structure preserving (ESP) control is used for additional damping injection, while using standard PD motor position control. The control method is applied for the first time to a flexible link robot by combining it with a link-side IMU-based observer. It is demonstrated in an industrial context using a standard controller setup, enabling straightforward implementation on existing industrial robots. The novel ESP method is further compared to a flatness-based control approach and to standard PD motor control. Particular aspects of controller tuning are discussed. Both theoretical analysis and experimental evaluations are conducted to address trajectory tracking behavior, disturbance rejection, and robustness to model parameter uncertainties. Results based on end effector accelerations show that ESP achieves superior vibration damping, demonstrating its effectiveness for industrial lightweight robots.**

***Index Terms*— flexible link robot, elastic structure preserving control, flatness-based control, extended Kalman filter**

I. Introduction

Control of flexible manipulators has been extensively studied since the 1970s, with numerous contributions in robotics and control theory [1]. In industrial robotics, elasticities primarily arose from the gears, leading to flexible joint models for model-based control. However, as robotic designs have evolved toward increased lightweight structures, structural link elasticities have become non-negligible [2].

This trend has created a continuous demand for improved mathematical modeling and control strategies to meet conflicting requirements, such as achieving high performance in weight-reduced robots with lower mechanical stiffness and increasingly complex vibration modes. Lightweight robots are highly susceptible to tool center point (TCP) oscillations from high jerk inputs and external disturbances, causing unacceptable positioning errors and long settling times, which are critical in industrial applications.

Industrial manipulators typically feature multiple links, with the upper arm and forearm being most relevant for structural flexibility. In this work, the Elastic Lightweight Arm (ElLA) from the JKU Linz Institute of Robotics (Fig. 1) serves as a benchmark platform due to its high compliance, making it well suited for vibration control studies.

While distributed mass models have been proposed for model based control, their complexity limits industrial adoption. Lumped element mass approaches, e.g. extended flexible link models [3], remain challenging for control tasks due to high dimensionality. Alternative modeling in [4] with control strategies such as strain feedback and wave echo control [5], have been shown to be effective, but rely on strain gauge measurements, which are less practical to retrofit in industrial context. A more feasible option is utilizing inertial measurement units (IMU) and approximating structural link flexibility through lumped element models with equivalent stiffness reduced to the joints. In [6] flatness-based trajectory control with vibration suppression using acceleration and angular rate measurements is introduced. This method has demonstrated successful on ElLA. However, it involves complex and non-intuitive controller parameterization due to variable stiffness resulting from reduced lumped element modeling.

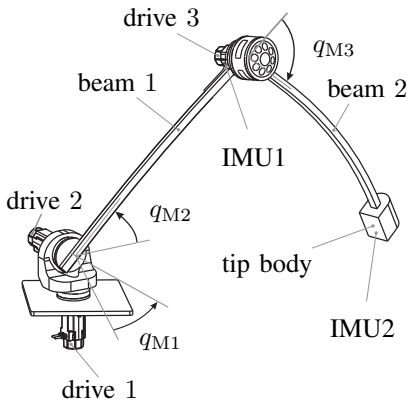

Fig. 1: Sketch of considered elastic robot ElLA.

Recent advances in control of variable stiffness actuators (VSA) for humanoid robots show promising results using a novel control scheme called elastic structure preserving (ESP) control [7]. The method achieves excellent tracking performance by model-based injection of link-side damping, enabling intuitive mutable vibration suppression. While initially tested only on elastic joint systems with link-side torque sensing, the elastic structure preserving approach is also promising for lightweight industrial manipulators. An initial proof-of-concept using ESP control for structurally elastic links was demonstrated in [8].

The contributions of this paper are

- Extension of the ESP control method to structurally elastic robots (elastic links and gears).
- Introduction of an observer to estimate the elastic state from IMU measurement, thus avoiding usage of link-

[1]Institute of Robotics, Johannes Kepler University Linz, Altenberger Str. 69, 4040 Linz, Austria {alexander.kitzinger, hubert.gattringer, a.mueller }@jku.at

side torque measurements, which are usually unavailable except for dedicated collaborative robots or are unreliable in case of flexible links.
- Amending the ESP control law to be applicable to position controlled industrial drives by means of path correction and auxiliary damping torque inputs, instead of direct torque commands. This is crucial for complying with safety frameworks of industrial controllers.
- Experimental results for a light-weight 3 DOF flexible-link robot. Results of the proposed ESP controller are compared with a flatness-based controller and a PD controller with non-linear feedforward. Their performance regarding trajectory tracking, disturbance rejection, and robustness to parameter variations is investigated. To this end, the robot was subjected to an unmodeled change of loads, one example involves collision with an obstacle.
- The important differences of the design/tuning of the above control schemes are highlighted with focus on their use with state-of-the-art industrial controller hardware.

II. Modeling

Fig. 1 depicts the mechanical setup of the elastic robot including two flexible beams and three harmonic drive gears actuated by synchronous motors. The maximum payload is $5\,\mathrm{kg}$ with a fully extended manipulator length of $2\,\mathrm{m}$. To monitor elastic vibrations triple-axis angular rate and acceleration sensors (IMU) are mounted on the elbow and end effector.

For model based control, a lumped element model is used, representing only virtual springs in base, shoulder and elbow joints. Hence gear and beam flexibility is reduced to the joints and torsional effects as well as strain along the beam axis is being neglected. The equivalent stiffness k_1, k_2, k_3 are shown in Fig. 2. It illustrates the front and top views of ElLA with the coordinate frames used for the three successive elementary rotations. The fixed inertial point is denoted by (I), and (E) corresponds to the end effector of the considered robot. Actuated joint angles are given by $\mathbf{q}_\mathrm{M}^\mathrm{T} = [q_{\mathrm{M}1}, q_{\mathrm{M}2}, q_{\mathrm{M}3}]$, while non-actuated angles are $\mathbf{q}_\mathrm{A}^\mathrm{T} = [q_{\mathrm{A}1}, q_{\mathrm{A}2}, q_{\mathrm{A}3}]$. The simplifications made yield a configuration-dependent stiffness $k_1(q_{\mathrm{A}2}, q_{\mathrm{A}3})$.

A. Equations of Motion

The formulation of the dynamics for the underactuated mechanical system is based on [9] and given by

$$\mathbf{M}_\mathrm{M}\ddot{\mathbf{q}}_\mathrm{M} + \mathbf{Q}_\mathrm{R}(\dot{\mathbf{q}}_\mathrm{M}) + \mathbf{K}(\mathbf{q}_\mathrm{A})(\mathbf{q}_\mathrm{M} - \mathbf{q}_\mathrm{A}) = \mathbf{Q}_\mathrm{M} \quad (1)$$

$$\mathbf{M}_\mathrm{A}(\mathbf{q}_\mathrm{A})\ddot{\mathbf{q}}_\mathrm{A} + \mathbf{C}_\mathrm{A}(\mathbf{q}_\mathrm{A}, \dot{\mathbf{q}}_\mathrm{A})\dot{\mathbf{q}}_\mathrm{A} + \mathbf{g}_\mathrm{A}(\mathbf{q}_\mathrm{A}) + \mathbf{K}(\mathbf{q}_\mathrm{A})(\mathbf{q}_\mathrm{A} - \mathbf{q}_\mathrm{M}) = \mathbf{0} \quad (2)$$

using the minimal coordinates of the three motor $\mathbf{q}_\mathrm{M}$ and their corresponding arm angles $\mathbf{q}_\mathrm{A}$. Inertial couplings and damping terms between motor and link coordinates are neglected ensuring the differential flatness of the system.

The positive definite, symmetric mass matrices $\mathbf{M}_\mathrm{M}$ and $\mathbf{M}_\mathrm{A}$ include the motor and arm inertia. Matrix $\mathbf{C}_\mathrm{A}$ accounts for Coriolis and centrifugal forces while $\mathbf{g}_\mathrm{A}$ is the gravitational force vector. Coupling between the actuated motor and under-actuated arm equation is represented by the diagonal and positive definite stiffness matrix $\mathbf{K}$. Vector $\mathbf{Q}_\mathrm{R}$ contains considered viscous and Coulomb friction, while $\mathbf{Q}_\mathrm{M} = \mathbf{B}_\mathrm{M}\boldsymbol{\tau}$ denotes generalized motor torques with gear transmission matrix $\mathbf{B}_\mathrm{M}$ and driving torques $\boldsymbol{\tau}$.

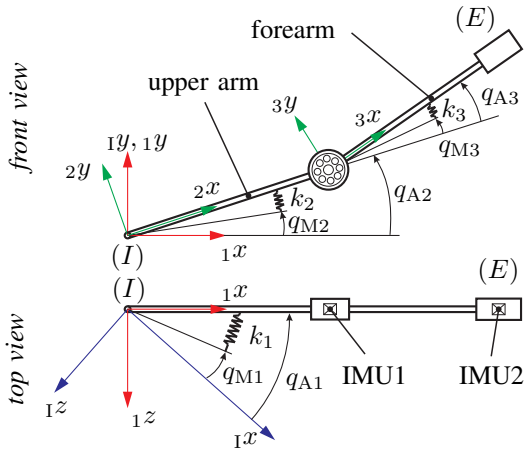

Fig. 2: Lumped element model with reduced equivalent stiffness to the joints.

B. Kinematics of Inertial Measurement Units

The IMUs measure angular velocity and translational acceleration at their mounting point. The measurements of both sensors can be related to the joint space using the Jacobian $\mathbf{J}(\mathbf{q}_\mathrm{A})$ of the forward kinematics for angular rate $\boldsymbol{\omega}_\mathrm{IMU}^\mathrm{T} = [\boldsymbol{\omega}_\mathrm{IMU1}^\mathrm{T}, \boldsymbol{\omega}_\mathrm{IMU2}^\mathrm{T}]$ and translational velocity $\mathbf{v}_\mathrm{IMU}^\mathrm{T} = [\mathbf{v}_\mathrm{IMU1}^\mathrm{T}, \mathbf{v}_\mathrm{IMU2}^\mathrm{T}]$ using the inertial frame

$$\begin{bmatrix} \boldsymbol{\omega}_\mathrm{IMU} \\ \mathbf{v}_\mathrm{IMU} \end{bmatrix} = \begin{bmatrix} \mathbf{J}_\omega(\mathbf{q}_\mathrm{A}) \\ \mathbf{J}_\mathrm{v}(\mathbf{q}_\mathrm{A}) \end{bmatrix} \dot{\mathbf{q}}_\mathrm{A} = \mathbf{J}(\mathbf{q}_\mathrm{A})\dot{\mathbf{q}}_\mathrm{A}. \quad (3)$$

Taking the time derivative of translational velocity and adding gravity $\mathbf{g}^\mathrm{T} = [0, -9.81, 0]$ in

$$\mathbf{a}_\mathrm{IMU} = \mathbf{J}_\mathrm{v}(\mathbf{q}_\mathrm{A})\,\ddot{\mathbf{q}}_\mathrm{A} + \dot{\mathbf{J}}_\mathrm{v}(\mathbf{q}_\mathrm{A})\,\dot{\mathbf{q}}_\mathrm{A} + \mathbf{g}. \quad (4)$$

yields the accelerations $\mathbf{a}_\mathrm{IMU}^\mathrm{T} = [\mathbf{a}_\mathrm{IMU1}^\mathrm{T}, \mathbf{a}_\mathrm{IMU2}^\mathrm{T}]$ expressed in the inertial frame.

III. Elastic State Observer

The elastic arm states $\mathbf{q}_\mathrm{A}, \dot{\mathbf{q}}_\mathrm{A}$ can be computed from IMU data algebraically with low computational effort [10] or estimated via an acceleration-based state observer [11]. In order to fully exploit sensor data, angular rate and acceleration measurements are fused using an Extended Kalman Filter (EKF) following [12]. The whole measurements used are motor position $\mathbf{q}_\mathrm{M}$, motor torque $\mathbf{Q}_\mathrm{M}$, angular rate $\boldsymbol{\omega}_\mathrm{IMU}$ and acceleration $\mathbf{a}_\mathrm{IMU}$. The only model information required is motor inertia $\mathbf{M}_\mathrm{M}$ and stiffness $\mathbf{K}$, meaning that no link parameters are needed.

Based on the state vector $\mathbf{x}^\mathrm{T} = [\mathbf{q}_\mathrm{M}^\mathrm{T}, \mathbf{q}_\mathrm{A}^\mathrm{T}, \dot{\mathbf{q}}_\mathrm{M}^\mathrm{T}, \dot{\mathbf{q}}_\mathrm{A}^\mathrm{T}] \in \mathbb{R}^{12}$ the time-discrete observer dynamic, using explicit Euler

method with sample time T_s, is given by

$$\mathbf{x}_{k+1} = (\mathbf{I} + T_\mathrm{s}\mathbf{A}_k)\,\mathbf{x}_k + T_\mathrm{s}\mathbf{B}\mathbf{Q}_{\mathrm{M},k} + T_\mathrm{s}\begin{bmatrix} \mathbf{0}^{9\times 1} \\ \ddot{\mathbf{q}}_{\mathrm{A},k} \end{bmatrix} + \mathbf{w}_k \tag{5}$$

using system matrix

$$\mathbf{A}_k = \begin{bmatrix} \mathbf{0} & \mathbf{0} & \mathbf{I} & \mathbf{0} \\ \mathbf{0} & \mathbf{0} & \mathbf{0} & \mathbf{I} \\ -\mathbf{M}_\mathrm{M}^{-1}\mathbf{K}(\mathbf{x}_{2,k}) & \mathbf{M}_\mathrm{M}^{-1}\mathbf{K}(\mathbf{x}_{2,k}) & \mathbf{0} & \mathbf{0} \\ \mathbf{0} & \mathbf{0} & \mathbf{0} & \mathbf{0} \end{bmatrix} \tag{6}$$

and input matrix

$$\mathbf{B}^\mathrm{T} = \begin{bmatrix} \mathbf{0} & \mathbf{0} & \mathbf{M}_\mathrm{M}^{-T} & \mathbf{0} \end{bmatrix}. \tag{7}$$

The calculation of vector $\ddot{\mathbf{q}}_{\mathrm{A},k}$ is based on (4) using the measured IMU accelerations

$$\ddot{\mathbf{q}}_{\mathrm{A},k} = \mathbf{J}_\mathrm{v}^\dagger\left(\mathbf{x}_{2,k}\right)\left(\mathbf{a}_{\mathrm{IMU},k} - \dot{\mathbf{J}}_\mathrm{v}\left(\mathbf{x}_{2,k}\right)\mathbf{x}_{4,k} - \mathbf{g}\right) \tag{8}$$

where $\mathbf{J}_\mathrm{v}^\dagger$ is the Moore–Penrose inverse. The measurement equation is

$$\mathbf{y}_k = \begin{bmatrix} \mathbf{x}_{1,k} \\ \mathbf{J}_\omega\left(\mathbf{x}_{2,k}\right)\mathbf{x}_{4,k} \end{bmatrix} + \mathbf{v}_k \tag{9}$$

with measurement vector $\mathbf{y}_k^\mathrm{T} = [\mathbf{q}_{\mathrm{M},k}^\mathrm{T}, \boldsymbol{\omega}_{\mathrm{IMU},k}^\mathrm{T}]$ including measured motor positions and angular velocities. The vector $\mathbf{w}_k$ represents added zero-mean process noise and $\mathbf{v}_k$ zero-mean measurement noise.

The EKF implementation follows the prediction and update steps in [13]. Explicit matrix inversion can be avoided in the error covariance prediction step by applying the derivative rule for matrix inversion when computing the Jacobian of (8). Parameter tuning to ensure convergence was carried out in accordance with [12].

IV. ESP vs. Flatness Based Control

This comparative study evaluates three control methods. The first implements the proposed ESP model-based vibration damping, while the second and third does not rely on model information for feedback control. In this work no friction compensation is applied, as its effect is mainly on static positional accuracy. The following sections briefly introduce each method, with control laws expressed in consistent notation to highlight differences.

A. Elastic Structure Preserving Control (ESP)

The control objective is to derive a structure preserving state transformation that transforms the underactuated system (1)–(2) into a quasi-full actuated closed loop form[1]

$$\mathbf{M}_\mathrm{M}\ddot{\tilde{\mathbf{q}}}_\mathrm{M} + \mathbf{K}(\tilde{\mathbf{q}}_\mathrm{M} - \tilde{\mathbf{q}}_\mathrm{A}) = \tilde{\mathbf{Q}}_\mathrm{M} \tag{10}$$

$$\mathbf{M}_\mathrm{A}\ddot{\tilde{\mathbf{q}}}_\mathrm{A} + \tilde{\mathbf{C}}_\mathrm{A}\dot{\tilde{\mathbf{q}}}_\mathrm{A} + \mathbf{K}(\tilde{\mathbf{q}}_\mathrm{A} - \tilde{\mathbf{q}}_\mathrm{M}) = -\mathbf{D}\dot{\tilde{\mathbf{q}}}_\mathrm{A} \tag{11}$$

where the adjustable positive definite diagonal-matrix $\mathbf{D}$ injects damping according to the new coordinates $\tilde{\mathbf{q}}^\mathrm{T} = [\tilde{\mathbf{q}}_\mathrm{M}^\mathrm{T}, \tilde{\mathbf{q}}_\mathrm{A}^\mathrm{T}]$ and new input $\tilde{\mathbf{Q}}_\mathrm{M}$. The new arm coordinates correspond to the motion error of the arm angles $\tilde{\mathbf{q}}_\mathrm{A} = \mathbf{q}_\mathrm{A} - \mathbf{q}_{\mathrm{A,d}}$ and the new motor coordinates $\tilde{\mathbf{q}}_\mathrm{M}$ reflect the desired damping and tracking behavior[2]. The transformation to the closed loop form (10)–(11) does not cause dynamical shaping of the inertia properties and preserves the initial stiffness $\mathbf{K}$ of the links. The gravitational and friction terms can be compensated, while Coriolis terms remain. Full derivations and detailed explanations, as well as stability and passivity proofs, are provided in [14].

The stiffness $\mathbf{K}(\mathbf{q}_\mathrm{A})$ and injected damping $\mathbf{D}(\mathbf{q}_\mathrm{A})$ depend on the robot configuration. However, as their rate of change is small, their time derivatives are neglected. Therefore, the control law for the generalized input torque can be decomposed into the following three components

$$\mathbf{Q}_\mathrm{M}^\mathrm{ESP} = \hat{\mathbf{Q}}_\mathrm{M}^\mathrm{ESP} + \check{\mathbf{Q}}_\mathrm{M}^\mathrm{ESP} + \tilde{\mathbf{Q}}_\mathrm{M}^\mathrm{ESP} \tag{12}$$

where the intermediate variables

$$\begin{aligned}\hat{\mathbf{Q}}_\mathrm{M}^\mathrm{ESP} =& \mathbf{M}_\mathrm{A}(\mathbf{q}_\mathrm{A})\ddot{\mathbf{q}}_{\mathrm{A,d}} + \mathbf{C}_\mathrm{A}(\mathbf{q}_\mathrm{A}, \dot{\mathbf{q}}_\mathrm{A})\dot{\mathbf{q}}_{\mathrm{A,d}} \\ &+ \mathbf{g}_\mathrm{A}(\mathbf{q}_\mathrm{A}) - \mathbf{D}\dot{\tilde{\mathbf{q}}}_\mathrm{A}\end{aligned} \tag{13}$$

$$\check{\mathbf{Q}}_\mathrm{M}^\mathrm{ESP} = \mathbf{M}_\mathrm{M}\ddot{\mathbf{q}}_{\mathrm{A,d}} + \mathbf{M}_\mathrm{M}\mathbf{K}^{-1}(\mathbf{q}_\mathrm{A})\frac{\mathrm{d}^2}{\mathrm{d}t^2}\hat{\mathbf{Q}}_\mathrm{M}^\mathrm{ESP} \tag{14}$$

conduct to the input transformation and

$$\tilde{\mathbf{Q}}_\mathrm{M}^\mathrm{ESP} = -\mathbf{K}_\mathrm{P}\tilde{\mathbf{q}}_\mathrm{M} - \mathbf{K}_\mathrm{D}\dot{\tilde{\mathbf{q}}}_\mathrm{M} \tag{15}$$

provides motor PD control in the new coordinates. The state transformation of the motor angle is given by

$$\mathbf{q}_\mathrm{M} = \tilde{\mathbf{q}}_\mathrm{M} + \mathbf{q}_{\mathrm{A,d}} + \mathbf{K}^{-1}(\mathbf{q}_\mathrm{A})\hat{\mathbf{Q}}_\mathrm{M}^\mathrm{ESP}. \tag{16}$$

Due to the use of position-based servo drives for the synchronous motors, the control law must be adapted based on the desired motor position

$$\mathbf{q}_{\mathrm{M,d}}^\mathrm{ESP} = \mathbf{q}_{\mathrm{A,d}} + \mathbf{K}^{-1}(\mathbf{q}_\mathrm{A})\hat{\mathbf{Q}}_\mathrm{M}^\mathrm{ESP} \tag{17}$$

in order to implement the decentralized motor PD control

$$\tilde{\mathbf{Q}}_\mathrm{M} = \mathbf{K}_\mathrm{P}(\mathbf{q}_{\mathrm{M,d}} - \mathbf{q}_\mathrm{M}) + \mathbf{K}_\mathrm{D}(\dot{\mathbf{q}}_{\mathrm{M,d}} - \dot{\mathbf{q}}_\mathrm{M}) \tag{18}$$

with positive definite feedback gains $\mathbf{K}_\mathrm{P}$ and $\mathbf{K}_\mathrm{D}$. The components $\hat{\mathbf{Q}}_\mathrm{M}^\mathrm{ESP}$ and $\check{\mathbf{Q}}_\mathrm{M}^\mathrm{ESP}$ can be applied using an additive torque in the servo drives as outlined in section VI.

B. Flatness Based Trajectory Control with Full State Error Feedback (FBC)

Differential flatness, well-defined in [15], facilitates model-based control of complex nonlinear systems. A flatness based representation of system (1)–(2) can be found in [6]. There, a flatness based trajectory control with arm angle and velocity feedback is used, also related in control theory as exact feedforward linearization with feedback of full state error vector. It combines a flatness-based feedforward torque and motor angle correction with two PD controllers stabilizing $\mathbf{q}_\mathrm{M}$ and $\mathbf{q}_\mathrm{A}$. To highlight the correlation to section (IV-A) a notation based on (12) is used.

The complete control law can be written as

$$\mathbf{Q}_\mathrm{M}^\mathrm{FBC} = \hat{\mathbf{Q}}_\mathrm{M}^\mathrm{FBC} + \check{\mathbf{Q}}_\mathrm{M}^\mathrm{FBC} + \tilde{\mathbf{Q}}_\mathrm{M} \tag{19}$$

[1]Due to compactness of the equations, arguments are not always denoted.

[2]Index d indicates desired arm angle $\mathbf{q}_{\mathrm{A,d}}$ and desired motor angle $\mathbf{q}_{\mathrm{M,d}}$.

with only using desired arm states in

$$\hat{\mathbf{Q}}_{\mathrm{M}}^{\mathrm{FBC}} = \hat{\mathbf{Q}}_{\mathrm{M}}^{\mathrm{ESP}}|_{\mathbf{q}_{\mathrm{A}}=\mathbf{q}_{\mathrm{A,d}}} \tag{20}$$

$$\check{\mathbf{Q}}_{\mathrm{M}}^{\mathrm{FBC}} = \check{\mathbf{Q}}_{\mathrm{M}}^{\mathrm{ESP}}|_{\mathbf{q}_{\mathrm{A}}=\mathbf{q}_{\mathrm{A,d}}} + \overline{\mathbf{Q}}_{\mathrm{M}} \tag{21}$$

and the additional PD arm feedback

$$\overline{\mathbf{Q}}_{\mathrm{M}} = \mathbf{K}_{\mathrm{PA}}(\mathbf{q}_{\mathrm{A,d}} - \mathbf{q}_{\mathrm{A}}) + \mathbf{K}_{\mathrm{DA}}(\dot{\mathbf{q}}_{\mathrm{A,d}} - \dot{\mathbf{q}}_{\mathrm{A}}). \tag{22}$$

By using only desired values in (13), (14) and (17) the model based damping injection $\mathbf{D}$ got eliminated. Passive vibration damping is archived with the feedforward torque and the desired motor coordinate

$$\mathbf{q}_{\mathrm{M,d}}^{\mathrm{FBC}} = \mathbf{q}_{\mathrm{A,d}} + \mathbf{K}^{-1}(\mathbf{q}_{\mathrm{A,d}})\hat{\mathbf{Q}}_{\mathrm{M}}^{\mathrm{FBC}} \tag{23}$$

while active vibration damping is realized via the additional feedback gains $\mathbf{K}_{\mathrm{PA}}$ and $\mathbf{K}_{\mathrm{DA}}$.

C. PD Motor Control with Feedforward Torque (PD)

As third method, simple flatness based PD motor control for the rigid-link model is evaluated as being the standard in most industrial robots. The control law

$$\mathbf{Q}_{\mathrm{M}}^{\mathrm{PD}} = \hat{\mathbf{Q}}_{\mathrm{M}}^{\mathrm{PD}} + \check{\mathbf{Q}}_{\mathrm{M}}^{\mathrm{PD}} + \tilde{\mathbf{Q}}_{\mathrm{M}} \tag{24}$$

can also be derived from (12) using feedforward terms under the assumption of $\mathbf{K}^{-1}$ converging towards zero. This results in $\mathbf{q}_{\mathrm{M,d}}^{\mathrm{PD}} = \mathbf{q}_{\mathrm{A,d}}$ and the feedforward torque

$$\hat{\mathbf{Q}}_{\mathrm{M}}^{\mathrm{PD}} = \hat{\mathbf{Q}}_{\mathrm{M}}^{\mathrm{ESP}}|_{\mathbf{q}_{\mathrm{A}}=\mathbf{q}_{\mathrm{A,d}}} \qquad \check{\mathbf{Q}}_{\mathrm{M}}^{\mathrm{PD}} = \mathbf{M}_{\mathrm{M}}\ddot{\mathbf{q}}_{\mathrm{A,d}}. \tag{25}$$

V. Damping Design by Modal Decomposition

A major advantage of ESP control is the model based injection of damping $\mathbf{D}$, enabling physically intuitive tuning. Beneficial is also that, due to the structure-preserving transformation, the closed-loop parameters are known from the beginning and motor and link-side damping can be tuned independently. In the following, the controller design for ElLA is presented under the assumption of negligible Coriolis and centrifugal terms.

A. Elastic Structure Preserving Control (ESP)

The adjustable parameters which determine the damping behavior of ESP control are link-side damping matrix $\mathbf{D}$ and motor controller gain $\mathbf{K}_{\mathrm{D}}$. They can be chosen based on the following modal decomposition.

Due to the assumptions made the quasi-full actuated system equation in closed loop form becomes

$$\mathbf{M}_{\mathrm{A}}(\mathbf{q}_{\mathrm{A}})\ddot{\tilde{\mathbf{q}}}_{\mathrm{A,d}} + \mathbf{D}(\mathbf{q}_{\mathrm{A}})\dot{\tilde{\mathbf{q}}}_{\mathrm{A}} + \mathbf{K}(\mathbf{q}_{\mathrm{A}})(\tilde{\mathbf{q}}_{\mathrm{A}} - \tilde{\mathbf{q}}_{\mathrm{M}}) = \mathbf{0}. \tag{26}$$

With the transformation $\tilde{\mathbf{q}}_{\mathrm{A}} = \mathbf{Y}_{\mathrm{A}}\mathbf{z}$ using $\mathbf{Y}_{\mathrm{A}} = [\mathbf{y}_1, \mathbf{y}_2, \mathbf{y}_3]$ representing the matrix of the eigenvectors $\mathbf{y}_{\mathrm{i}}$ of eigenvalues λ_{i} according to

$$\left[\mathbf{M}_{\mathrm{A}}\lambda_{\mathrm{i}}^2 + \mathbf{D}\lambda_{\mathrm{i}} + \mathbf{K}\right]\mathbf{y}_{\mathrm{i}}e^{\lambda_{\mathrm{i}}t} = \mathbf{0} \tag{27}$$

equation (26) can be transformed into the modal space

$$\mathbf{Y}_{\mathrm{A}}^{\mathrm{T}}\mathbf{M}_{\mathrm{A}}\mathbf{Y}_{\mathrm{A}}\ddot{\mathbf{z}} + \mathbf{Y}_{\mathrm{A}}^{\mathrm{T}}\mathbf{D}\mathbf{Y}_{\mathrm{A}}\dot{\mathbf{z}} + \mathbf{Y}_{\mathrm{A}}^{\mathrm{T}}\mathbf{K}\mathbf{Y}_{\mathrm{A}}\mathbf{z} = \mathbf{0} \tag{28}$$

resulting in a system of n decoupled equations. When comparing the system to the standard second-order form

$$\ddot{\mathbf{z}} + 2\mathbf{D}_{\xi}\mathbf{\Lambda}^{1/2}\dot{\mathbf{z}} + \mathbf{\Lambda}\mathbf{z} = \mathbf{0} \tag{29}$$

using $\mathbf{\Lambda} = \mathbf{Y}_{\mathrm{A}}^{-1}\mathbf{M}_{\mathrm{A}}^{-1}\mathbf{K}\mathbf{Y}_{\mathrm{A}}$ it becomes evident that modal damping can be set through

$$\mathbf{D} = 2\mathbf{M}_{\mathrm{A}}\mathbf{Y}_{\mathrm{A}}\mathbf{D}_{\xi}\left(\mathbf{Y}_{\mathrm{A}}^{-1}\mathbf{M}_{\mathrm{A}}^{-1}\mathbf{K}\mathbf{Y}_{\mathrm{A}}\right)^{1/2}\mathbf{Y}_{\mathrm{A}}^{-1} \tag{30}$$

where diagonal matrix $\mathbf{D}_{\xi}$ contains the modal damping factors $\xi_{\mathrm{i}} \in [0, 1]$ as elements.

An analogous approach can be applied for selecting $\mathbf{K}_{\mathrm{D}}$ by considering the actuated closed-loop dynamics

$$\mathbf{M}_{\mathrm{M}}\ddot{\tilde{\mathbf{q}}}_{\mathrm{M}} + \mathbf{K}_{\mathrm{D}}\dot{\tilde{\mathbf{q}}}_{\mathrm{M}} + \mathbf{K}(\mathbf{q}_{\mathrm{A}})(\tilde{\mathbf{q}}_{\mathrm{M}} - \tilde{\mathbf{q}}_{\mathrm{A}}) + \mathbf{K}_{\mathrm{P}}\tilde{\mathbf{q}}_{\mathrm{M}} = \mathbf{0} \tag{31}$$

which yields

$$\mathbf{K}_{\mathrm{D}} = 2\mathbf{M}_{\mathrm{M}}\mathbf{Y}_{\mathrm{M}}\mathbf{K}_{\mathrm{D}_{\xi}}\left(\mathbf{Y}_{\mathrm{M}}^{-1}\mathbf{M}_{\mathrm{M}}^{-1}(\mathbf{K} + \mathbf{K}_{\mathrm{P}})\mathbf{Y}_{\mathrm{M}}\right)^{1/2}\mathbf{Y}_{\mathrm{M}}^{-1} \tag{32}$$

with $\mathbf{K}_{\mathrm{P}}$ denoting the pre-determined proportional gain. $\mathbf{Y}_{\mathrm{M}}$ again represents the modal decomposition matrix, and $\mathbf{K}_{\mathrm{D}_{\xi}}$ the diagonal modal damping matrix of the motor side.

To ensure the desired modal damping throughout the robot's workspace, the parameters $\mathbf{D}$ and $\mathbf{K}_{\mathrm{D}}$ must be adapted in each control cycle. Since the inertia matrices are positive definite and $\mathbf{K}$ is symmetric, the modal decomposition – and consequently the damping parameterization – can be computed efficiently using Cholesky decomposition.

B. Flatness Based Trajectory Control with Full State Error Feedback (FBC)

Since the closed loop form of the flatness based control with full state error feedback is not as quasi-full actuated as in case of ESP control, the damping of the actuated and underactuated system dynamics cannot be tuned independently. When fixed PD motor controller parameters are used and only the vibration damping behavior is to be adjusted, the parameterization of the controller becomes challenging. To address this issue, [16] proposes an Interconnection and Damping Assignment - Passivity Based Control (IDA-PBC), which could be used to provide at least certain restrictions on the control parameters to support systematic tuning.

For the experimental results presented in VII, the motor-side gains $\mathbf{K}_{\mathrm{P}}$ and $\mathbf{K}_{\mathrm{D}}$ are chosen to be the same as in ESP control, while the feedback gains for the observed arm angle, $\mathbf{K}_{\mathrm{PA}}$ and $\mathbf{K}_{\mathrm{DA}}$, are experimentally tuned for optimal performance.

C. PD Motor Control with Feedforward Torque (PD)

In the case of simple PD control, the gains $\mathbf{K}_{\mathrm{P}}$ and $\mathbf{K}_{\mathrm{D}}$ are selected analogously to those of the other control methods, which enables a direct comparison, as no additional damping is applied.

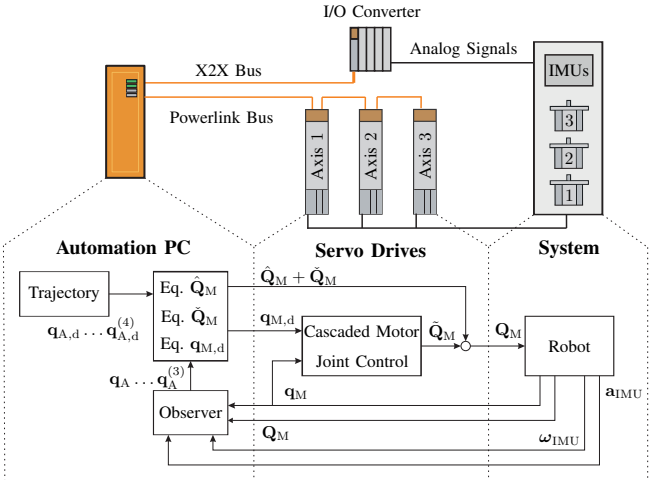

Fig. 3: Industrial controller setup with an illustration of the control scheme including the dedicated decentralized position control implemented on the servo drives.

VI. Experimental Setup

The mechanical setup of the considered elastic robot was already introduced in section II. The electrical setup, including the main components of the control loop, is shown in Fig. 3. A central computing unit (automation PC) with a cycle time of $400\,\mu\mathrm{s}$ communicates with the servo drives via an Ethernet Powerlink bus. The IMUs are connected to the central computing unit via I/O converters. Each servo drive contains a cascaded position control loop consisting of position, velocity, and current control units. The only available measurements are the encoder signals, providing the current motor angle $\mathbf{q}_\mathrm{M}$. Settable target values are restricted to desired motor angles $\mathbf{q}_\mathrm{M,d}$, which means that all velocities in the servo drive must be obtained numerically by time differentiation.

To realize the desired model-based vibration damping, the additional input torques are computed centrally on the automation PC, transmitted via the bus system, and superimposed on the torques from the decentralized position controller in the servo drives. For each control method, the corresponding additive torque is calculated according to the equations in section IV and integrated as depicted in Fig. 3. It is important to point out that the additional torque is designed to improve tracking performance without any effect on existing safety mechanisms, such as built-in lag error monitoring.

A. Issues for Practical Implementation

Although critical damping can theoretically be achieved, several practical limitations restrict the maximum attainable modal damping factor. Since the lumped-element model represents only the first eigenmode, higher-order vibration frequencies must be suppressed in the IMU signals. In addition, high-frequency disturbances – primarily caused by torque ripple in the harmonic drive gears and amplified by structural flexibility – are sensed by the angular velocity and acceleration sensors ([17], [18]). These disturbances are attenuated through low-pass filtering in the I/O converters, which introduces time delay and reduces phase margins. Furthermore, modeling uncertainties and the numerical computation of the third time derivative of the arm angle must be taken into account. For these reasons, the modal link-side damping applied in the experiments was limited to $\xi_\mathrm{i} = 0.3$.

TABLE I: Controller parameters used during experiments.

$\mathbf{K}_\mathrm{P}$	$\mathrm{diag}(30\mathrm{e}3, 30\mathrm{e}3, 30\mathrm{e}3)$	$\mathbf{K}_\mathrm{D}$	$\mathrm{diag}(399, 665, 618)$
$\mathbf{D}_\xi$	$\mathrm{diag}(0.3, 0.3, 0.3)$	$\mathbf{K}_{\mathrm{D}_\xi}$	$\mathrm{diag}(0.7, 0.7, 0.7)$
$\mathbf{K}_\mathrm{PA}$	$-\mathrm{diag}(10\mathrm{e}3, 12\mathrm{e}3, 800)$	$\mathbf{K}_\mathrm{DA}$	$\mathrm{diag}(250, 368, 64)$

B. Time-Optimal Trajectory

To evaluate the controllers under high-dynamic conditions, the experiments were based on a time-optimal point-to-point trajectory calculated using the lumped element model. The trajectory starts at point $\mathbf{r}_\mathrm{A}^\mathrm{T} = [1.4, -0.5, -0.75]$ and ends at point $\mathbf{r}_\mathrm{B}^\mathrm{T} = [1.4, 1.0, 0.75]$ as shown in Fig. 4. The optimization objective follows the formulation in [19].

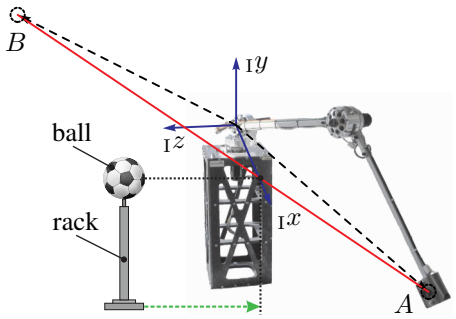

Fig. 4: Test setup with a ball on a rack which can be placed into the trajectory path for simulating external disturbances.

C. Control Parameters

The proportional motor gain was set manually such that none of the control inputs overshoot the maximal motor torque of $\tau_\mathrm{max} = 3.5\,\mathrm{Nm}$. All other parameters are determined following section V. Since the servo drive restricts $\mathbf{K}_\mathrm{D}$ to a fixed value that cannot be adapted depending on the workspace, the modal damping was set at operating point B in Fig. 4. The complete set of controller parameters used in the experiments is summarized in Table I. Throughout all experiments, the controller parameters for each control method were kept the same.

VII. Comparative Study Results

As the main objective is reducing elastic vibrations a comparison with focus on TCP accelerations is made. First, the tracking performance with respect to the acceleration reference is evaluated. Second, external disturbances are introduced by placing a $0.42\,\mathrm{kg}$ ball loosely in the end effector path using a rack, as illustrated in Fig. 4. In the third experiment, metal plates up to $1.5\,\mathrm{kg}$ are removed from the tip body to demonstrate the effect of model uncertainties. A multimedia attachment accompanies this paper and demonstrates the experimental setup and key results.

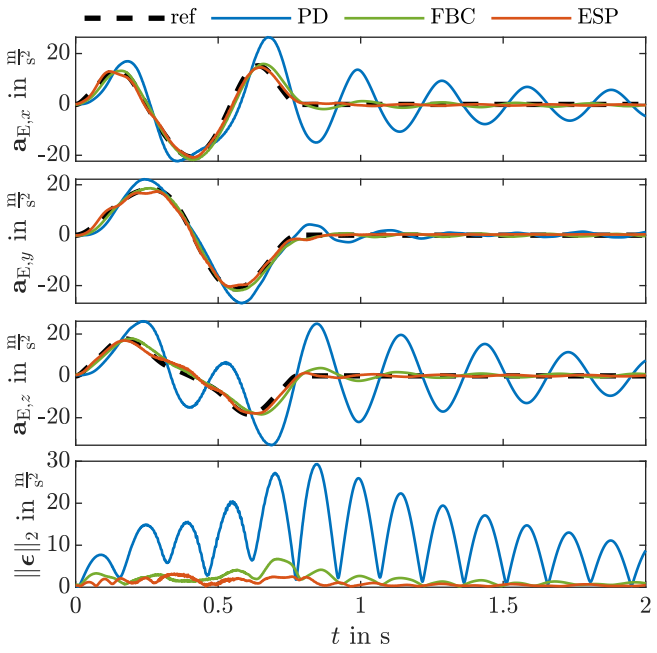

Fig. 5: Tracking performance of the robot. Shown are the translational accelerations of the end effector.

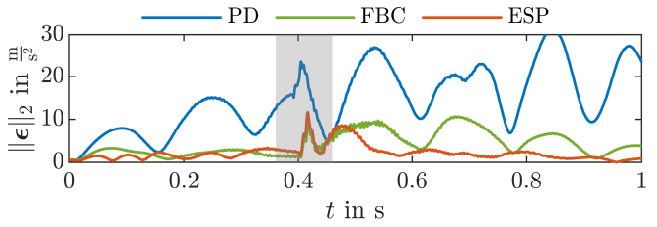

Fig. 6: Tracking performance under disturbance, with the highlighted area indicating the time of external impact.

A. Tracking Performance

Fig. 5 shows a comparison of the tracking performance using the end-effector acceleration $\mathbf{a}_{\mathrm{E}}$ in each Cartesian direction and the corresponding Euclidean error $\|\boldsymbol{\epsilon}\|_2 = \|\mathbf{a}_{\mathrm{E}} - \mathbf{a}_{\mathrm{E,d}}\|_2$. The trajectory terminates after $0.78\,\mathrm{s}$, after which the robot oscillates around the final position. The ESP control scheme achieves the best performance, remaining close to the reference throughout and after the trajectory. The flatness-based approach also performs well but exhibits slightly higher vibrations in the stationary phase. The PD controller performs worst, as it provides neither additional passive nor active vibration damping.

B. External Disturbances

The ball was placed for all three control methods at the same position in the workspace, causing an impact along the trajectory at approximately $0.4\,\mathrm{s}$ after the start. The resulting tracking error is shown in Fig. 6, where the impact peaks are clearly visible. The ESP control method again achieves the best performance, as the oscillations induced by the ball impact decay most rapidly. Comparison with the undisturbed case in Fig. 5 requires noting the different time-axis scaling.

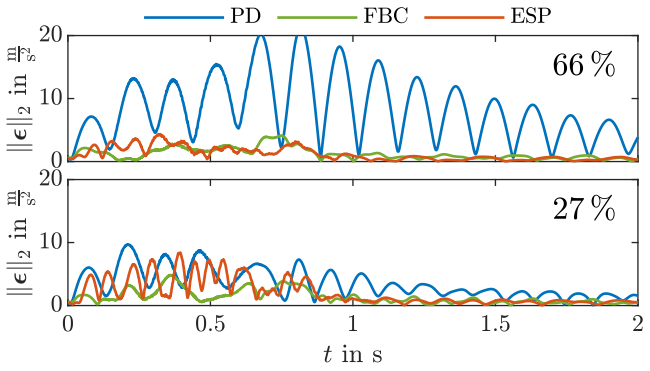

Fig. 7: Tracking performance of the robot with reduced end effector mass noted in percent to the initial value.

C. Effect of Model Uncertainties

Since ESP relies on model parameters for feedback control, unlike FBC and PD, its sensitivity to model errors is of special interest. To evaluate this, the robot end-effector mass was reduced in two stages (from $100\,\%$ to $66\,\%$ and $27\,\%$) without adapting any model or controller parameters. The resulting tracking behavior, again expressed as acceleration lag errors, is shown in Fig. 7. With decreasing end-effector mass, elastic deflections and thus oscillation amplitudes are reduced, allowing PD control to approach the more advanced methods in tracking performance. Nevertheless, ESP and FBC achieve superior vibration suppression, as tip body accelerations decay more rapidly after finishing the trajectory. As model error increases, FBC outperforms ESP, as it does not rely on model information for feedback control, revealing potential for adaptive parameter estimation in ESP.

VIII. Conclusions

The experimental results demonstrate that ESP control is feasible for structurally elastic robots in combination with a link-side IMU-based observer. In addition, results were achieved that exceeded FBC commonly applied in industrial vibration damping, and clearly surpasses PD, confirming the necessity of vibration suppression for elastic lightweight robots. ESP achieves the best tracking and disturbance rejection performance, but at the cost of higher complexity, as it stronger relies on observed elastic states and model information. However, controller parameterization and damping design for fixed position control parameters is much easier. In summary, this comparative study provides theoretical and experimental insights into benefits of ESP, FBC, and PD, offering a foundation for selecting suitable control concepts in industrial context.

Future research should focus on a theoretical analysis of sensitivity to model and control parameters. Moreover, the lumped element model should be extended to capture higher-order vibration modes, while torque ripples from harmonic drives should be mitigated, e.g. following [20].

Acknowledgment

This work was supported by the LCM – K2 Center for Symbiotic Mechatronics within the framework of the Austrian COMET-K2 program.

REFERENCES

[1] M. Sayahkarajy, Z. Mohamed, and A. A. Mohd Faudzi, "Review of modelling and control of flexible-link manipulators," *Proceedings of the Institution of Mechanical Engineers, Part I: Journal of Systems and Control Engineering*, vol. 230, no. 8, pp. 861–873, 2016.

[2] A. De Luca, "Feedforward/feedback laws for the control of flexible robots," in *Proceedings 2000 ICRA. Millennium Conference. IEEE International Conference on Robotics and Automation. Symposia Proceedings*, vol. 1, 2000, pp. 233–240.

[3] S. Moberg, E. Wernholt, S. Hanssen, and T. Brogårdh, "Modeling and parameter estimation of robot manipulators using extended flexible joint models," *Journal of Dynamic Systems, Measurement, and Control*, vol. 136, no. 3, 2014.

[4] J. Malzahn, R. F. Reinhart, and T. Bertram, "Dynamics identification of a damped multi elastic link robot arm under gravity," in *2014 IEEE International Conference on Robotics and Automation (ICRA)*, 2014, pp. 2170–2175.

[5] J. Malzahn and T. Bertram, "On the equivalence of direct strain feedback and lumped parameter wave echo control for oscillation damping of elastic-link arms," *IEEE Robotics and Automation Letters*, vol. 1, no. 1, pp. 447–454, 2016.

[6] P. Staufer, H. Gattringer, and H. Bremer, "Vibration suppression for a flexible link robot using acceleration and/or angular rate measurements and a flatness based trajectory control," in *International Design Engineering Technical Conferences and Computers and Information in Engineering Conference*, vol. 54839, 2011, pp. 1101–1110.

[7] M. Keppler, D. Lakatos, C. Ott, and A. Albu-Schäffer, "Elastic structure preserving (esp) control for compliantly actuated robots," *IEEE Transactions on Robotics*, vol. 34, no. 2, pp. 317–335, 2018.

[8] A. Kitzinger, H. Gattringer, and A. Müller, "Elastic structure preserving control for a structurally elastic robot," in *Austrian Robotics Workshop*, 2025.

[9] H. Bremer, *Elastic Multibody Dynamics - A Direct Ritz Approach*, ser. Intelligent Systems, Control and Automation: Science and Engineering. Heidelberg: Springer Verlag, 2008, vol. 35.

[10] P. Staufer and H. Gattringer, "State estimation on flexible robots using accelerometers and angular rate sensors," *Mechatronics*, vol. 2012, pp. 1043–1049, 2012.

[11] A. De Luca, D. Schroder, and M. Thummel, "An acceleration-based state observer for robot manipulators with elastic joints," in *Proceedings 2007 IEEE International Conference on Robotics and Automation*, 2007, pp. 3817–3823.

[12] M. Reyhani, L. Marko, G. Janisch, and A. Kugi, "Real-time observer designs for elastic-joint industrial robots: Experimental comparison and new strategies," *Mechatronics*, vol. 99, p. 103140, 2024.

[13] C. A. Lightcap and S. A. Banks, "An extended kalman filter for real-time estimation and control of a rigid-link flexible-joint manipulator," *IEEE Transactions on Control Systems Technology*, vol. 18, no. 1, pp. 91–103, 2010.

[14] M. Keppler, "From underactuation to quasi-full actuation: A unifying control framework for rigid and elastic joint robots," Ph.D. dissertation, Technical University of Munich, 2023.

[15] M. van Nieuwstadt, M. Rathinam, and R. M. Murray, "Differential flatness and absolute equivalence of nonlinear control systems," *SIAM Journal on Control and Optimization*, vol. 36, no. 4, pp. 1225–1239, 1998.

[16] P. Staufer, "Ein Beitrag zur Regelung von strukturelastischen Mehrkörpersystemen," Ph.D. dissertation, Johannes Kepler Universität Linz, 2012.

[17] F. H. Ghorbel, P. S. Gandhi, and F. Alpeter, "On the kinematic error in harmonic drive gears," *Journal of Mechanical Design*, vol. 123, no. 1, pp. 90–97, 1998.

[18] T. Hidaka, T. Ishida, Y. Zhang, M. Sassahara, and Y. Tanioka, "Vibration of a strain wave gearing in an industrial robot," in *Proceedings of the 1990 International Power Transmission and Gearing Conference —New Technology Power Transmission*, 1990, pp. 789–794.

[19] K. Springer, H. Gattringer, and P. Staufer, "On time-optimal trajectory planning for a flexible link robot," *Proceedings of the Institution of Mechanical Engineers, Part I: Journal of Systems and Control Eng.*, vol. 227, no. 10, pp. 751–762, 2013.

[20] M. Iwasaki and H. Nakamura, "Vibration suppression for angular transmission errors in harmonic drive gearings and application to industrial robots," *IFAC Proceedings Volumes*, vol. 47, no. 3, pp. 6831–6836, 2014.